SURFACE EROSION OF PLASMA-FACING MATERIALS USING AN ELECTROTHERMAL PLASMA SOURCE AND ION BEAM MICRO-TRENCHES

J. D. Coburn[1], T. E. Gebhart[2], C. M. Parish[2], E. Unterberg[2], J. Canik[2],

M. W. Barsoum[3], M. Bourham[1]

[1]*North Carolina State University, Raleigh, NC.* jdcoburn@ncsu.edu

[2]*Oak Ridge National Laboratory, Oak Ridge, TN.*

[3]*Drexel University, Philadelphia, PA.*

Dr. Mohamed Bourham

1122 Burlington Engineering Laboratory

2500 Stinson Drive

Raleigh, NC 27695-7909

# of pages: ?? (6103 words)

# of tables: 3

# of figures: 14

SURFACE EROSION OF PLASMA-FACING MATERIALS USING AN ELECTROTHERMAL PLASMA SOURCE AND ION BEAM MICRO-TRENCHES

J. D. Coburn[1], T. E. Gebhart[2], C. M. Parish[2], E. Unterberg[2], J. Canik[2],

M. W. Barsoum[3], M. Bourham[1]

[1]North Carolina State University, Raleigh, NC. jdcoburn@ncsu.edu

[2]Oak Ridge National Laboratory, Oak Ridge, TN.

[3]Drexel University, Philadelphia, PA.

Abstract

Erosion characteristics of tungsten-alternative plasma-facing materials were tested under high heat flux conditions in the electrothermal (ET) plasma source facility at Oak Ridge National laboratory. The plasma-facing materials of interest are high-purity β-3C CVD silicon carbide and the MAX phases Ti_3SiC_2 and Ti_2AlC. An erosion analysis method was developed using a combination of focused ion beam microscopy and scanning electron microscopy, carving micro-trench geometries into polished sample surfaces. Samples of SiC, Ti_3SiC_2 and Ti_2AlC were exposed to the ET plasma source along-side tungsten and monocrystalline silicon. Samples were exposed to a Lexan polycarbonate ($C_{16}H_{14}O_3$) ET plasma stream in a He environment, at a specified impact angle, with IR camera diagnostics. ELM-relevant heat fluxes of 0.9 – 1 GW/m^2 over 1 ms discharges were generated on the target surfaces. Tungsten samples exhibited pronounced melt-layer formation and deformation, with measured molten pits 2 – 10 μm in diameter and melt-layer depths of up to 7 μm deep. Surface erosion rates for Ti_3SiC_2 and Ti_2AlC ranged from 80 – 775 μm/s and 85 – 470 μm/s, respectively. Both MAX phases exhibited extreme surface fracture and material ejection, with damage depths past 4 μm for Ti_2AlC and 11

μm for Ti_3SiC_2. SiC displayed the best performance, in one case surviving 15 consecutive ET plasma exposures with an average erosion rate of about 29 μm/s and no surface fracturing. SiC erosion rates ranged from 23 – 128 μm/s.

I. Introduction

Plasma-facing materials (PFMs) in future large-scale fusion reactors must be designed to protect structural components while dissipating extreme thermal loads. While JET and other mid-size tokamaks experience minimal erosion of PFMs, ITER will be the first large-scale tokamak to experience significant net erosion due to its high power, long pulse operations. Normal operating scenarios will involve large but manageable PFM heat loads on the order of 0.25-10 MW/m^2 [1,2]. Of greater concern is heat flux driven erosion from off-normal transient events, which grow in severity with reactor size due to the increased plasma stored energy. Materials must withstand high heat fluxes from events such as edge localized modes (ELMs), vertical displacement events (VDEs), and thermal quench phases of plasma disruptions. Uncontrolled type I ELMs and disruptions on ITER, for example, are capable of producing ~GW/m^2 heat fluxes during $Q_{DT} = 10$ operations [3,4]. Such severe conditions will lead to extensive material erosion through melting, bubbling, splattering or direct evaporation and sublimation, spreading aerosols and particulates of eroded material throughout the reactor vessel. Additionally, ion bombardment will cause substantial erosion due to physical surface sputtering, and neutron/ion damage within the bulk material can lead to component failure. PFM solutions past ITER will require a unique balance of properties in order to handle high heat loads while maximizing PFM lifetime and minimizing impurity loss.

This experimental work focuses on the erosive behavior of alternative, innovative PFMs when exposed to plasma jets from an electrothermal (ET) plasma source, operated at Oak Ridge National Laboratory (ORNL). Candidate materials SiC, Ti_3SiC_2, and Ti_2AlC were exposed alongside W and Si to single and multiple ET plasma jets. The objective was to compare each material's erosion characteristics under ELM- and disruption-relevant heat flux conditions of ~GW/m^2, determining which material erodes the least in a melt- or sublimation-dominated regime. This experiment complements a recent plasma exposure experiment performed at the DIII-D National Fusion Facility which studied the same PFMs under a physical sputtering-dominated erosion regime with ~MW/m^2 heat fluxes [5]. In order to evaluate the total net erosion and damage on the solid sample surfaces, a new technique using state-of-the-art microscopy was developed.

II. Experiment Information

II.A Plasma-Facing Material Candidates

A class of materials known as MAX phase ceramics offer promise as candidate PFMs. These ceramics are layered compounds with a chemical formula $M_{n+1}AX_n$, where M is an early transition metal (such as Ti or Ta), A is an A-group element (such as Si or Al), and X is carbon or nitrogen [6]. The near close-packed M-X layers are interwoven with purely A-group layers into a hexagonal crystal structures. Due to this layered structure, the MAX phases bulk mechanical properties do not match expectations of MX material: they are easily machinable, fatigue resistant, thermal shock resistant, and relatively damage tolerant [6]. Some also exhibit high thermal and electrical conductivities for ceramics, ideal for exhausting high heat loads. The MAX phases are relatively new to research for nuclear applications, with a handful of radiation tolerance studies for fission applications and with few published exposures to plasma sources.

Recent works [7,8,9] analyzing the irradiation properties of a few commercially available MAX phases highlight Ti_3SiC_2 and Ti_2AlC as promising candidates for nuclear environments. Although this experiment focuses on high heat flux erosion characteristics, strong radiation resistance is an equally important property of next-generation PFMs, making Ti_3SiC_2 and Ti_2AlC ideal subjects for the first ET plasma exposure of MAX phase ceramics. The MAX samples used in this work were prepared from the same sources as reference [5], manufactured and supplied by Drexel University.

The other PFM of interest is silicon carbide, SiC, a material of continued interest to both fission and fusion nuclear research. Single crystal SiC is a ceramic with a combination of desirable PFM properties, including a high sublimation point at ~2700 °C, high thermal conductivity and temperature tolerance, good plasma compatibility due to a low average Z, and good material integrity under neutron irradiation [10,11,12]. SiC sublimates rather than melts, and it is non-magnetic which minimizes eddy/halo current forces due to disruptions. A major drawback of monolithic SiC is its inherent brittleness, which compromises its use as a structural material [12]. For polycrystalline SiC, the crystal structure, grain size, density, and purity will affect the average mechanical and thermal properties. These characteristics can be varied based on the fabrication process used. Much progress has been made in the past two decades designing SiC/SiC composites with improved mechanical properties [10,12,13]. There have also been improvements in the manufacturing processes of bulk, polycrystalline SiC using chemical vapor deposition (CVD), generating high purity samples with no voids or microcracks [14]. For this experiment, bulk CVD SiC samples were manufactured in order to test both their erosion rates and their improved robustness under tokamak plasma exposures. The SiC is Rohm & Haas CVD,

β-3C, at 99.9995% purity with a 5 μm grain size at a density of 3.21 g/cc [14], the same as in reference [5].

II.B Electrothermal Plasma Source

An electrothermal (ET) plasma source is a pulsed capillary plasma discharge that operates in the confined ablative arc regime. The source consists of an electrode, an ablating liner, and a ground housing with source insulation. Charge is stored on a capacitor and then discharged through a spark gap switch, after which the arcing current through the source induces Joule heating and ablation of the liner material from radiative heat transport. The resulting plasma jet typically has temperatures on the order of 1-5 eV and an electron density on the order of $10^{22} – 10^{28}$ /m^3, depending on the magnitude of the discharge current. Most importantly, ET sources are capable of producing ~GW/m^2 heat fluxes, both on the liner material via radiation heat flux and at the barrel exit via the resulting plasma jet [15 – 18]. Such a capability makes ET sources suitable for simulating ELM and disruption impacts for reactor-relevant plasma material interaction studies. General descriptions of ET plasma source operations can be found in the literature, including details on the specific ET source operated at Oak Ridge National Laboratory (ORNL) that was used for this study [15].

Specific details for this experiment setup are as follows. The ET source has an adaptable pulse-forming network in the electrical system along with multiple options for 'liner sleeves' and target plate holders. A current pulse length of 1ms was selected, relevant to long ELMs and short plasma disruptions. Lexan brand polycarbonate "$C_{16}H_{14}O_3$" [15] liners were chosen since they are well tested in ET discharges. Post-experiment surface depositions from the Lexan were also relatively easy to clean without damaging the exposed samples. The source is backfilled with helium gas to 40-60 Torr right before each discharge. Thus the resultant plasma impacting the

target is a combination of C, H, O, and He ions. To measure the corresponding heat flux, the ET source housing can accommodate an infrared (IR) camera viewing port. The plasma generated by the current pulse impacts a target plate that is angled 45° with respect to the axis of the plasma jet. The target plate holds the prepared PFM samples at the center of the jet impact area and is angled in this way to accommodate the IR camera viewing angle. Coincidentally, a ~45° ion impact angle is more realistic than a normal incidence for a divertor environment [19,20]. It should be noted that many ET material erosion studies in the literature [16,18,21] analyze the heat flux on, and mass loss of, the liner material. The radiant heat flux in this case is comprised of photons from the Joule heating effect of the core plasma. Again, this experiment focuses on material samples placed at the end of the ET source barrel, such that the heat flux and erosion are due to impact of ions, electrons, and hot neutrals from the plasma jet.

II.C Focused Ion Beam Micro-Trench Technique

Non-destructive, post-mortem techniques are essential for measuring the net erosion thickness loss on PFM samples. A unique analysis method was developed specifically for larger, bulk samples that are more representative of plasma-facing components, the same technique utilized in the correlated experiment in reference [5]. A focused ion beam (FIB) is used to carve micrometer-scale trenches into polished sample surfaces for erosion loss measurements. The depth of each micro-trench is characterized using scanning electron microscopy (SEM), as well as atomic force microscopy (AFM) if the micro-trench is shallow enough. An angled plasma flux will impact the divertor surface during tokamak operations [19,20], motivating the angled sample orientation described in Section II.B. As the top surface of the samples erodes during the angled plasma exposure, certain walls of the micro-trenches will be shadowed from any particle flux due to their orientation. Thus, each micro-trench is also designed with fiducial depth markings

etched into the shadowed trench walls. The integrated, post-exposure changes in trench geometry combined with time-dependent ET source diagnostics provide a measure of the net erosion rate for each material. The post-exposure thickness loss can be determined by either 1) measuring the shadowed fiducial depth markings with SEM imaging, or 2) measuring the new height difference between the sample surface and trench floor with a SEM or AFM.

FIB markings have been increasingly used in the plasma-material interactions community for erosion studies, such as in references [22, 23]. The unique, innovative aspects of the technique used here lie in the detailed micro-trench preparation and the post-experiment analysis method. Instead of etching FIB geometries or markers on a macroscopically cut edge, the micro-trench geometry is carved into a flat, uniformly polished material surface. The shape, orientation, and depth of the micro-trench are optimized in order to view surface erosion along the micro-trench edge. The FIB micro-trench design for the ET samples is slightly different than that used in [5]. Multiple preliminary exposures were performed to help discern the appropriate micro-trench geometries and cleaning methods. Under ~GW/m^2 heat fluxes, it was expected that microns of material may be eroded from some sample surfaces, especially for multi-shot exposures. Test exposures on aluminum and stainless-steel samples at lower heat flux values confirmed this expectation. The final geometry iteration is depicted in Figure 1, a 10 μm wide x 12 μm long trench at least 10 μm deep. The micro-trench length and width settings were based on manufacturing time and angled imaging requirements. Due to the depth being > 5 μm, AFM analysis could not be used.

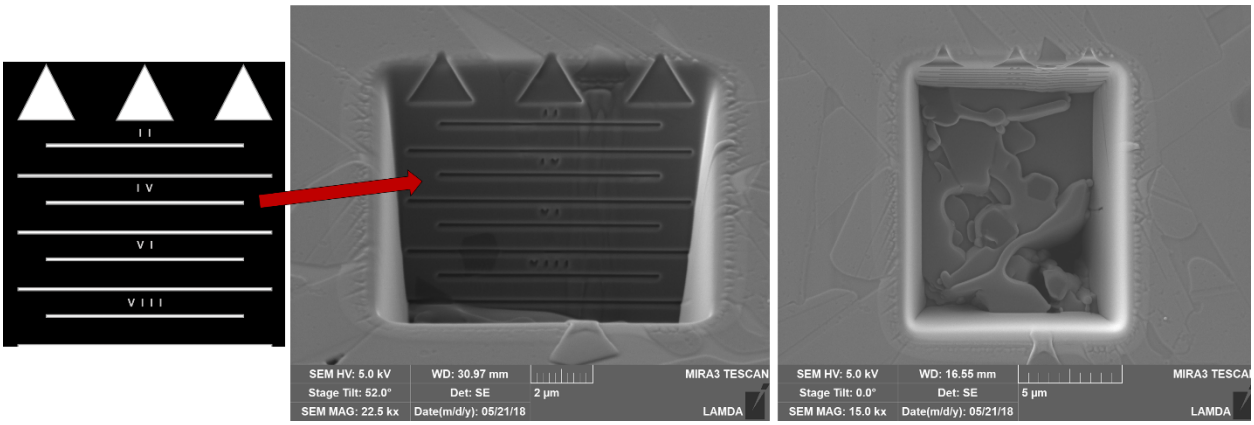

Figure 1 – (Left) The FIB bitmap image used to mark the depth within the micro-trench, up to 10 µm. The triangles are 2 µm long, and each line is spaced 1 µm apart. (Middle) SEM image of an example 10 x 12 µm micro-trench in Ti_2AlC, displaying the bitmap depth markings etched into the shadowed micro-trench wall at a 52° angle. (Right) The same micro-trench from a top-down, 0° angle view.

To increase the accuracy of the SEM image depth measurements, a bitmap image was carved into the shadowed micro-trench wall. The finalized bitmap image is displayed in Figure 1 on the left. Triangular shapes were utilized as in [5] to account for rounding effects on the trench edges. Lines were then added to extend the measurement capabilities up to depths of 10 µm. Roman numeral markings were included as well, for cases where some markings at the top and/or bottom become indiscernible and it is necessary to locally identify each line. During FIB manufacturing, the bitmap is scaled such that each triangle is programmed to be 2 µm deep, while each line is spaced 1 µm apart, totaling to a marked depth of 10 µm. The scaling accounts for the 38° milling angle, corresponding to the physical angle of the FIB relative to the surface parallel, and represents a 10 µm deep image milled onto a perfectly vertical wall. Unfortunately, the micro-trench walls are not geometrically perfect, with noticeable rounding of the top edges

and slight sloping of the walls. This characteristic causes the depth markings to be milled at slightly more shallow depths than desired. Thus, a two-image measurement technique must be utilized for accurate depth calculations rather than relying directly on the fiducial markings. Details of the two-image measurement method are documented in reference [5].

For sample preparation, all samples were polished at ORNL using colloidal silica (1-5 nm particle size) to a mirror finish. After being manufactured and polished, each sample was cleaned via an ultrasonic cleaner with acetone, ethanol, and methanol (~2 minutes per solution), after which they were plasma cleaned via an Ar-O plasma for 5 to 10 minutes. Only after this cleaning process were the samples loaded into a FIB for micro-trench manufacturing and characterization. Post-experiment, the samples were cleaned as described previously via the ultrasonic and plasma cleaners before SEM imaging. This step was necessary to remove hydrocarbon ash from the ET source that would often fill the micro-trenches and obscure the fiducial depth markings.

III. Experiment Results

All three PFMs of interest, Ti_3SiC_2, Ti_2AlC, and SiC, were exposed alongside samples of Si and W that were available. Samples were manufactured at the same time as those for the DIII-D experiment in [5], from the same material sources. They have a cylindrical geometry with a flat, 6 mm diameter surface exposed to the ET plasma. Some were thin, 1.6 mm thick samples while others were of the larger 6 mm thick geometry. This dimensional difference was solely the consequence of availability. A custom carbon steel holder was manufactured to hold the samples within the ET source vacuum chamber, exposing only the circular 6mm diameter surface to incoming plasma flux.

A total of 15 samples were prepared for the ET experiment. Micro-trenches were placed in three distinct locations 2mm apart from one another, such that the effects of a radially varying

heat flux would be observed. A shot plan was developed to expose each material to 2 – 3 different heat flux values by also varying the voltage difference, ΔV, across the ET capacitor circuit between 6 – 7 kV. A timescale of 1000 – 1200 μs was achieved for all ET discharges, relevant to long ELMs and short disruptions. At least one sample of each PFM was also exposed to multiple shots.

III.A Heat Flux Analysis

A FLIR IR camera was used to collect temperature data of the sample surface during exposure. The IR camera viewed the sample holder through a small sapphire window, with the sample oriented at about a 45° angle. The camera produces a 2-D matrix of temperature data at a maximum 1337 Hz. This rate captured on average 2-3 frames where the plasma jet visibly struck the target. Figure 2 shows a series of raw frames from the IR camera that depict the evolution of the plasma jet impact. As the plasma jet exits the ET source barrel on the right and travels left, it hits the target and sample at a 45° angle, heating the sample surface as the plasma jet spreads outwards due to the impact.

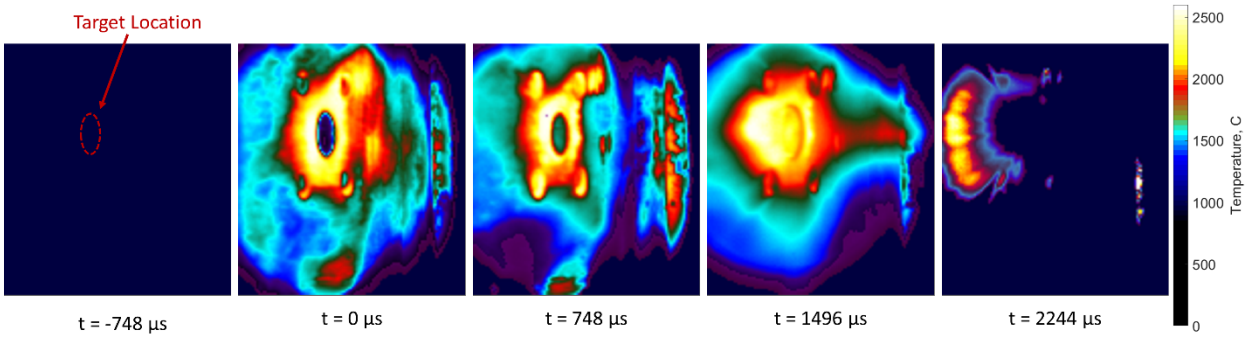

Figure 2 – A time-lapse of raw IR temperature data frames on a SiC sample. The plasma jet is shot from the ET source barrel on the right of each frame, travelling from right to left until impact is made on the angled target holder.

The measured emissivity of each material sample is displayed in Table 1. Measurements were performed ~300°C before exposure, and all samples displayed lower than normal emissivities due to their surface polish [24]. IR signal loss through the sapphire window was also accounted for in the final surface temperature calculation assuming an IR transmission efficiency of 0.87. The constant heat flux impinging on the ET samples was then estimated using the IR temperature data using a 1-D model. Figure 3 shows a photo of a sample housed in the target holder after plasma exposure along with an example heat flux map. The impact and flow of the plasma jet onto the holder can be inferred from the deposition pattern of hydrocarbon ash. Since the PFM samples possessed different emissivity values and thermal properties than the carbon steel holder, the sample was usually discernable in the IR thermal data. 4 screw holes around the sample were also usually visible.

Table 1 – Summary of Measured Sample Emissivities

MATERIAL	EMISSIVITY (FRACTION)
SIC	0.34
TI_3SIC_2	0.17
TI_2ALC	0.19
SI	0.27
W	0.15

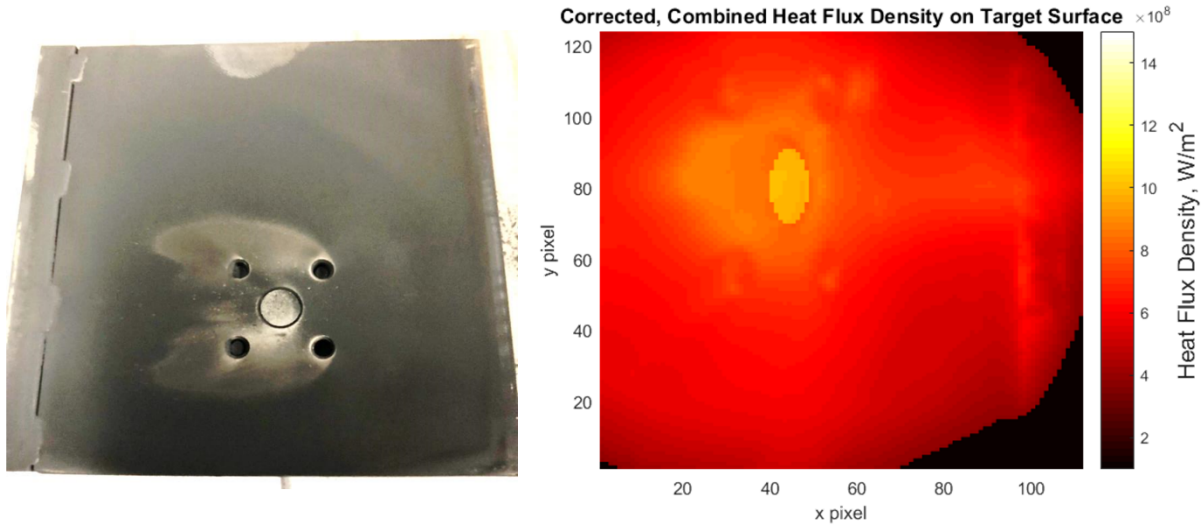

Figure 3 – (Left) Post-exposure image of the ET target holder with a SiC sample, uncleaned (Right) Heat flux density calculated from the T_R temperature map, calculated separately for a SiC sample and the carbon steel holder. The central temperature is ~1850 °C for the SiC sample, resulting in a corresponding heat flux calculation of ~1 GW/m^2.

Unfortunately, experimental complications hindered the ability to generate a substantial heat flux dataset. For all exposures, only a general statement on the heat flux can be confidently made: samples experienced an average of 0.9 – 1 GW/m^2 with standard deviations on the order of 5 – 10%.

III.B Microscopy Analysis

The metal, ceramic, and monocrystalline materials exhibited qualitatively different surface responses. In the test sample of monocrystalline Si, signs of extreme melting and boiling are visible along with deep surface fracturing, as displayed in Figure 4. The additional erosion mechanism of material ejection due to surface fracture complicated the microscopy analysis. The materials Ti_3SiC_2, Ti_2AlC, and Si all exhibited fracturing into the micro-trench wall itself, which

may or may not correspond to the fracture depths seen on the polished surface. This complication necessitated two different erosion depth measurements: the average erosion depth experienced by the total surface, Δt_s, and the average erosion depth of cracks into the micro-trench, Δt_c, measured with respect to the new eroded surface height. For the original goals of the study, Δt_s is the quantity of interest. Figure 5 highlights the relationship between Δt_s and Δt_c in a Si test sample where there is clear material loss from the average surface in addition to cracks propagating into the micro-trench geometry.

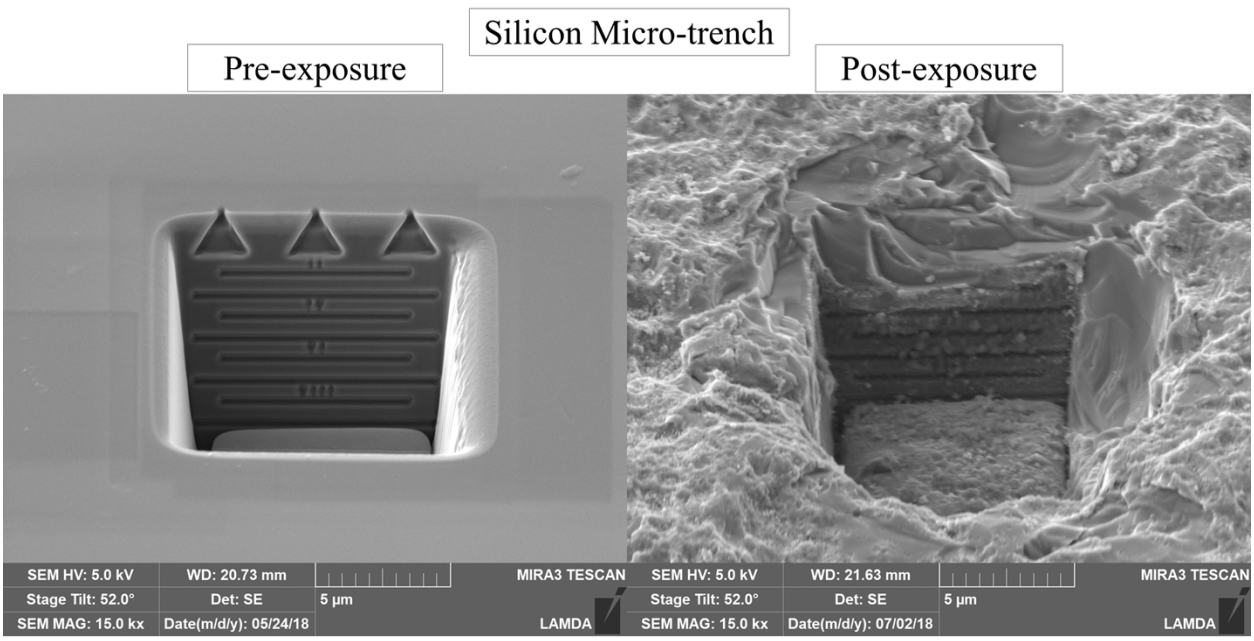

Figure 4 – (Left) Example Si micro-trench, pre-exposure, at a 52° angled view. (Right) Si micro-trench after being exposed to one ET plasma shot at a programmed 6 kV.

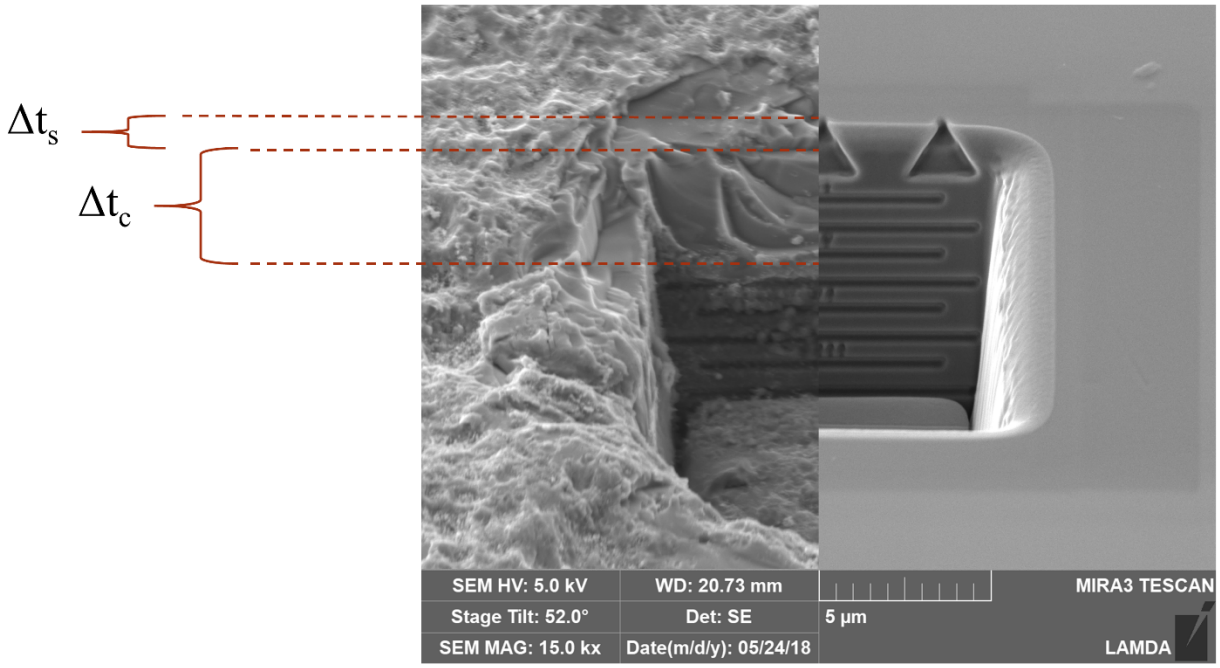

Figure 5 – Overlaid images of a Si micro-trench for post-exposure (Left) and pre-exposure (Right).

III.B.i Tungsten

Two tungsten, W, samples were exposed during the experiment. One saw a single plasma shot at a programmed 6 kV, while the other was exposed to a series of 5 plasma shots at 6kV. Although there is no specific ITER-grade of W, these W samples met "ITER-grade" requirements. Thus, the W results represent the standard to which the alternative materials should be compared, at least in regards to their use as divertor PFMs. With such high melting and boiling points (3422 and 5930 °C, respectively), it was unknown whether the ET pulse would be sufficient to reach a sublimation-dominated erosion regime for W. Significant melting and melt-layer motion was observed on the surfaces for both the 1 shot and 5 shot cases, consistent with expectations from [1,3,21]. Figure 6 depicts pre- and post-experiment SEM

images of the two W surfaces, highlighting the extreme degradation of the material surface with consecutive plasma exposures.

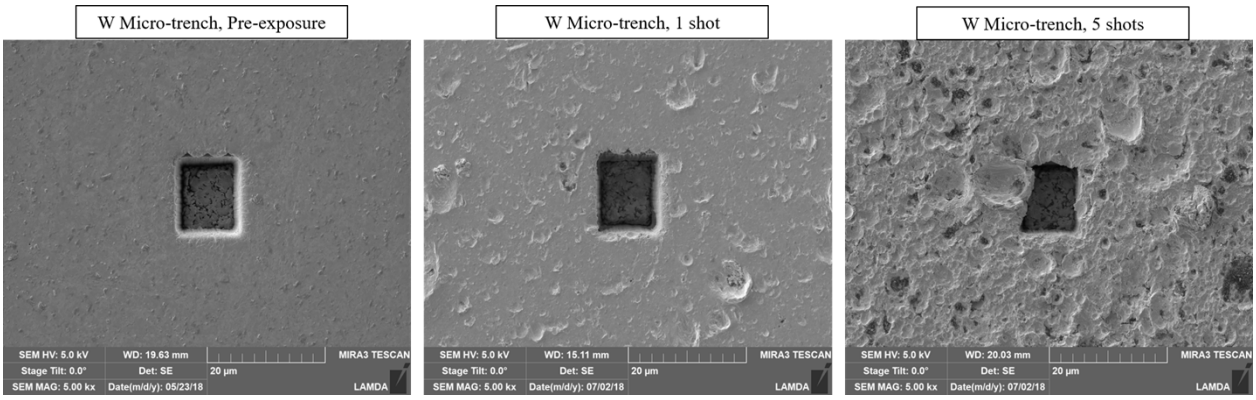

Figure 6 – (Left) Example W micro-trench, pre-exposure, at a 0° top-down view. (Middle) W micro-trench after being exposed to one ET plasma shot at a programmed 6 kV. (Right) W micro-trench after being exposed to 5 consecutive shots at 6 kV.

In the case of one ET plasma exposure, the molten pits were uniformly dispersed over the sample surface and varied in size from 2 – 5 µm in diameter. They do not constitute the entire surface, implying that any material loss is localized. Multiple melting pits along the micro-trench edge provided depth estimations of about 1-2 µm, highlighted in Fig. 7. EDX analysis confirmed that the molten features were tungsten, with traces of hydrocarbon ash impurities sometimes present in uncleaned craters. Based on deformation of micro-trench fiducial markings, the melt layer penetrated a maximum of 2 µm into the surface. There was no significant melt-layer motion or deformation of the micro-trench geometry. The individual molten pits, however, do exhibit melt motion and re-solidification in the plasma flow direction.

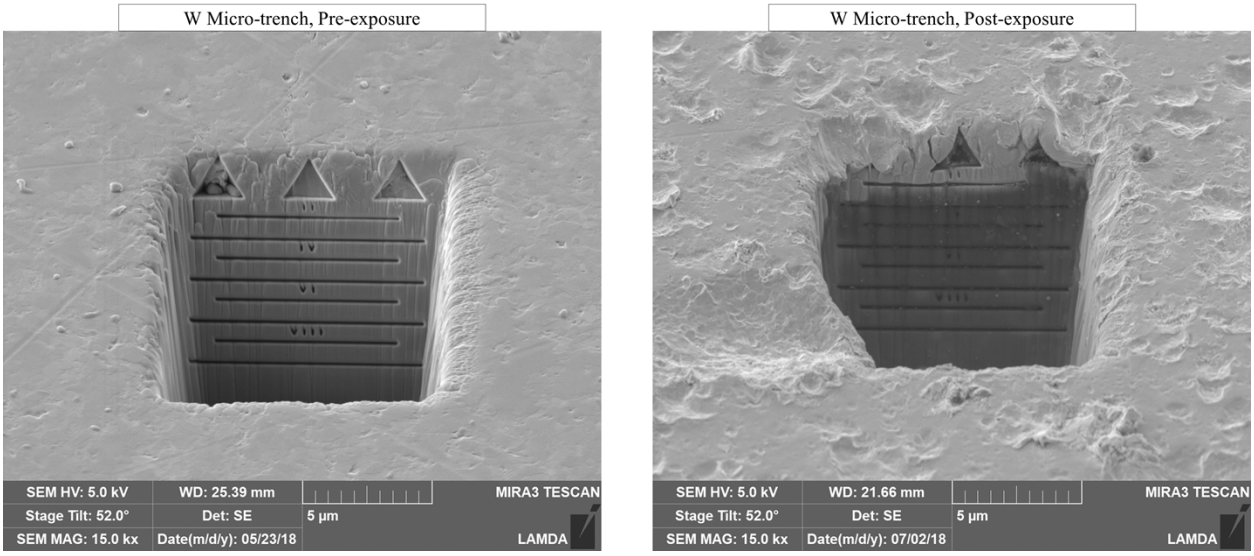

Figure 7 - Pre-exposure (Left) and post-exposure (Right) images of an example micro-trench in W exposed to one 6 kV ET plasma discharge, viewed at a 52° tilt.

The surface melt layer that formed from the 5-shot exposure was more extreme and uniform than the 1-shot case. The molten pits are larger in size, up to 10 µm in diameter, and all blend together to comprise a fully deformed surface. Repeated plasma exposures appear to have grown the molten pits with each successive shot, as well as induced significant melt-layer motion of the entire surface. Of the three micro-trenches available to observe on the 5-shot sample, only one remained suitable for obtaining erosion measurements and is displayed in Fig. 8. Significant deformation of the micro-trench structure and the corresponding fiducial markings is observed, with only the middle triangle marking being suitable for depth measurements. As seen in the upper right image of Fig. 8, the melt layer penetrated a maximum of 7 µm into the surface. Another W micro-trench exhibited a cascade of the melt-layer into the trench, hindering the image-based measurement technique. The third micro-trench was backfilled with a mass of molten W

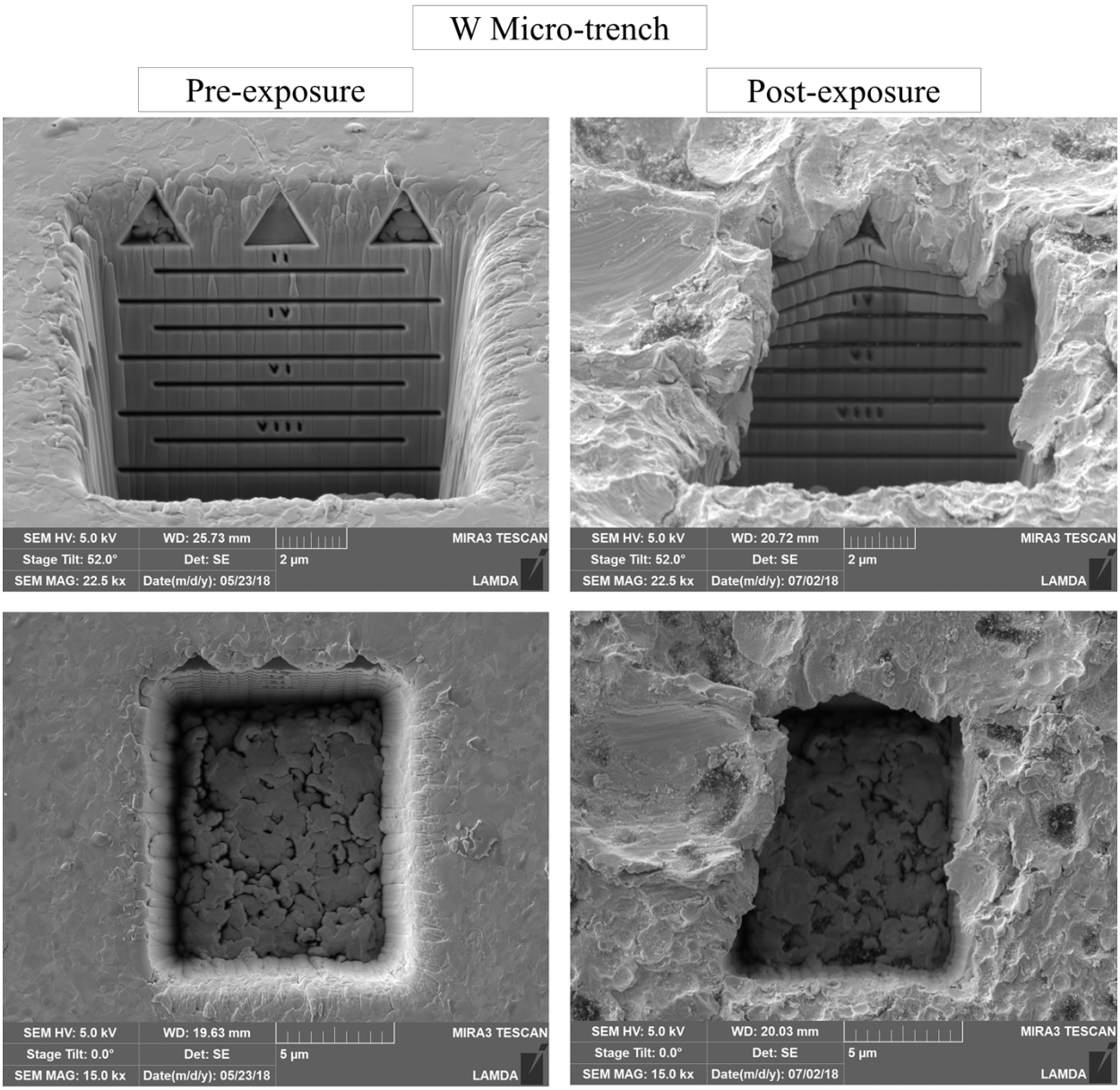

Figure 8 - Pre-exposure (Left) and post-exposure (Right) images of an example micro-trench in W exposed to 5 consecutive, 6 kV ET plasma discharges, viewed at a 52° tilt (top images) and a top-down 0° tilt (bottom images).

III.B.ii Ti_3SiC_2

Three Ti_3SiC_2 samples were exposed during the experiment, one to a series of 5 plasma shots at 6 kV and the other two exposed to single 6kV and 7 kV shots. The post-exposure

Ti_3SiC_2 samples exhibited an apparent combination of melting, boiling, and surface fracturing. Small, scattered molten pits were observed for the 1 shot cases, ranging from 0.1 – 1.5 μm in diameter. Deep fracturing of the Ti_3SiC_2 material resulted in the formation of jagged, sharp holes and crevices as fractured material was presumably ejected from the surface. EDX analysis was performed on the samples to attempt to measure any dissociation that may have occurred, particularly a loss of the A-group element Si. Ti, Si, and C were uniformly seen across the surface, implying that the molten/deformed material is bulk Ti_3SiC_2. Some deformation of the edge geometry was observed, i.e. bending and elongation, however a clear layer of melt motion was not visible. Bulk fracturing along the trench edges made it difficult to make depth measurements for the average material surface. In some cases, entire portions of the micro-trench wall were observed to have fractured and collapsed within the micro-trench. Figure 9 highlights an example where material loss due to surface melting and from fracturing are both observed along the micro-trench edge.

In the case of the consecutive 5-shot ET exposure, uniform fracturing and erosion loss was observed on the sample surface and along each micro-trench wall. As fracture sites are generated during successive plasma shots, they propagate from one another, resulting in a uniformly jagged and eroded material surface. Consequently, the amount of fracturing and material loss on the micro-trench walls was more severe than in the 1-shot case. In one instance, erosion spanned past the maximum 10 μm FIB depth markings. It was important to take depth measurements for both the average surface height and for the fracture depth within the micro-trench wall. Figure 10 is another overlaid image meant to highlight the depth of fracturing observed in the 5-shot Ti_3SiC_2 sample.

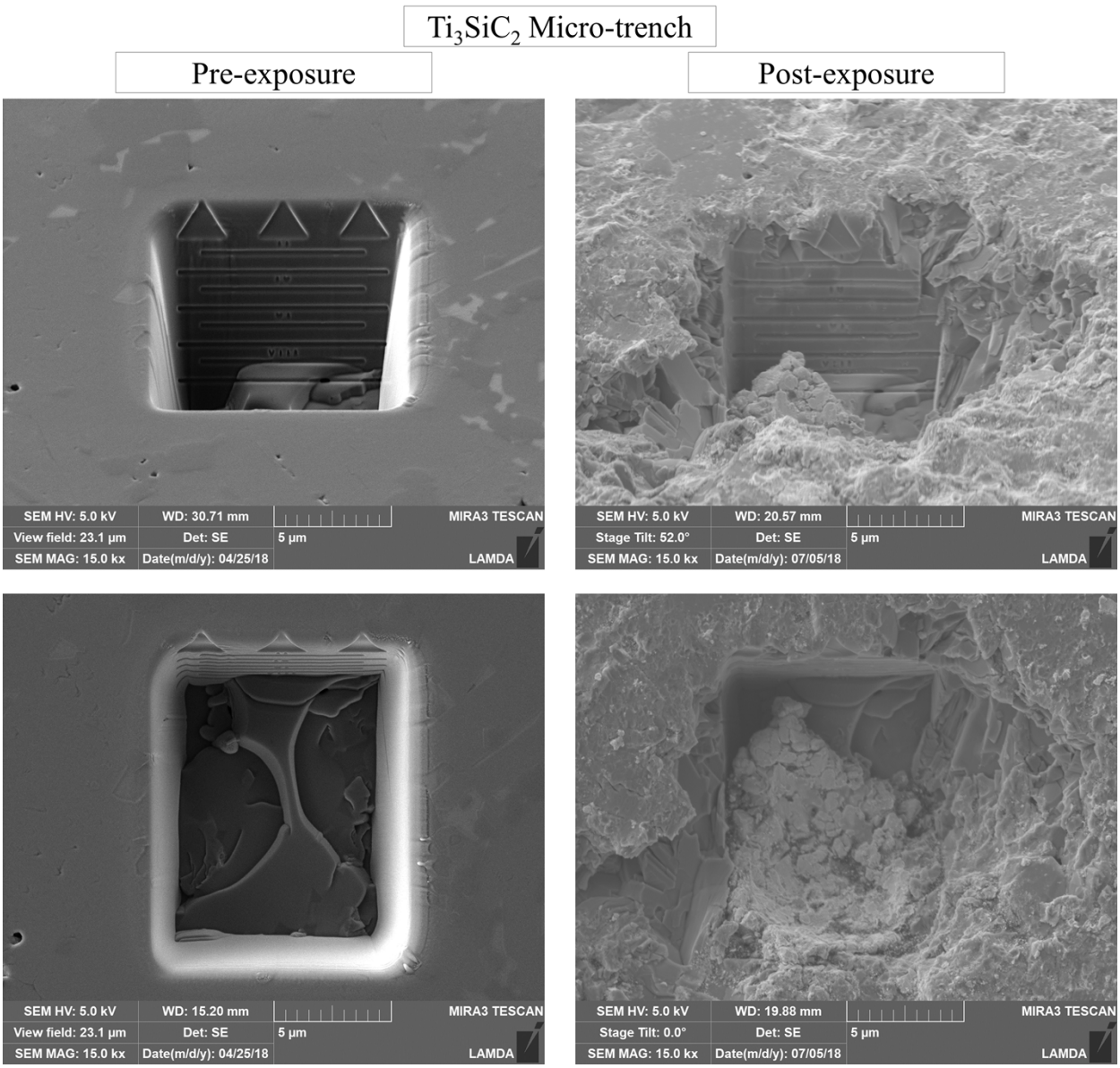

Figure 9 – Pre-exposure (Left) and post-exposure (Right) images of an example micro-trench in Ti_3SiC_2 exposed to one 7kV ET plasma discharge, viewed at a 52° tilt (top images) and a top-down 0° tilt (bottom images).

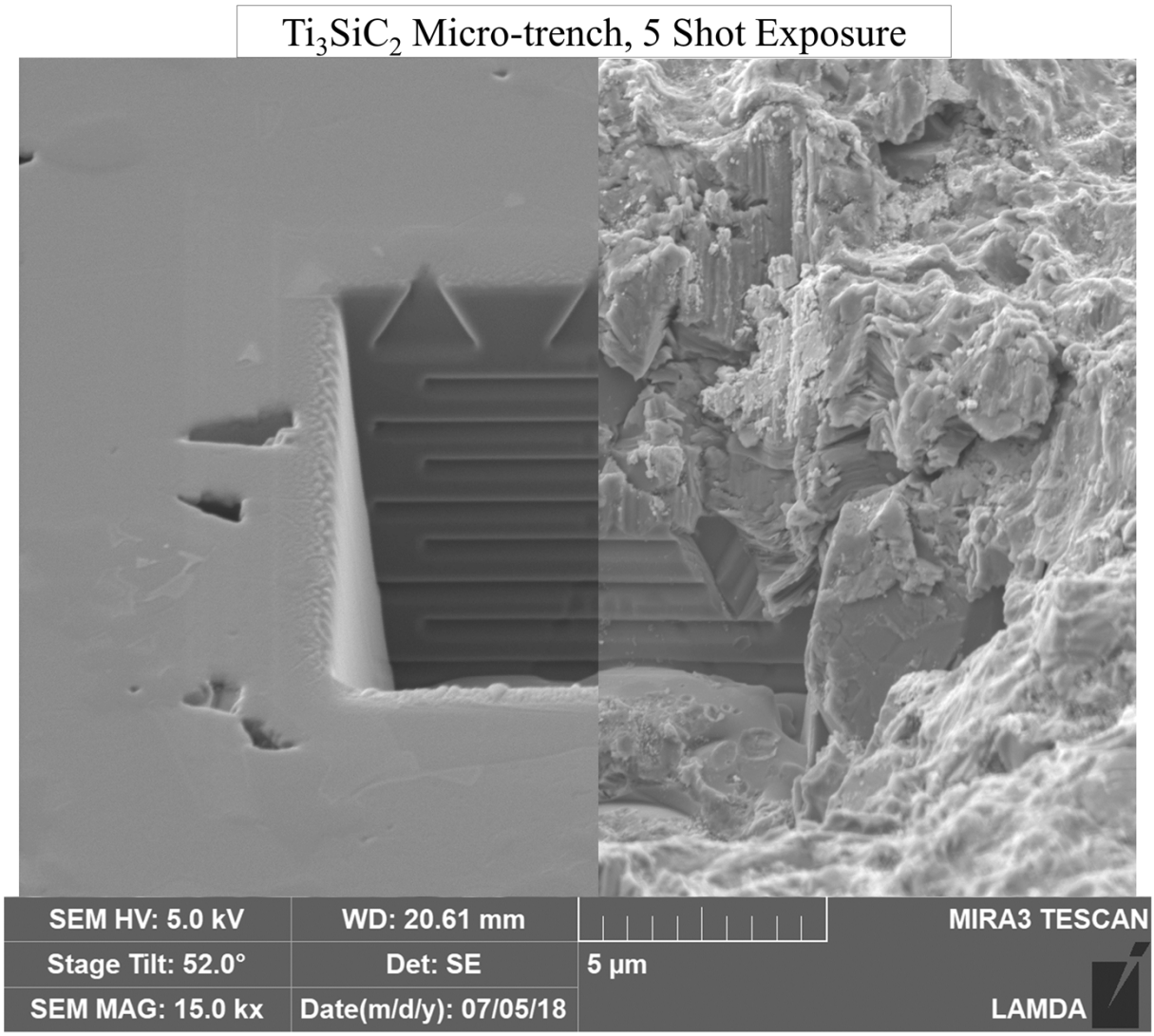

Figure 10 - Overlaid images of a Ti_3SiC_2 micro-trench for pre-exposure (Left) and post-exposure (Right), highlighting fracturing of the micro-trench wall down to the 9 µm depth marker.

III.B.iii Ti_2AlC

Four Ti_2AlC samples were exposed during the experimental campaign, with three exposed to a single plasma shot at a programmed ΔV of 6 kV, 6.5 kV, and 7 kV and one exposed to 5 consecutive plasma shots at 6 kV. The samples exhibited a combination of melting, boiling, and surface fracturing. Small, scattered molten pits were observed for the 1-shot and 5-shot

cases. These pits were of the same scale as those observed on the Ti_3SiC_2 samples, ranging from about 0.1 – 1 μm in diameter. In the case of single ET plasma exposures, relatively uniform erosion from the melting/boiling pits was observed on the micro-trench edges. An apparent shallow melt layer was observed along the edges, often < 1 μm deep. Fracturing and material ejection was observed in some Ti_2AlC samples but to a much less severe extent than in Ti_3SiC_2. Most were shallow fractures < 4 μm deep. Qualitatively, fracture effects did appear slightly more severe with increasing heat flux, especially the depth of visible cracks that did not necessarily result in material ejection. Figure 11 is an overlaid image that provides a good example of uniform melt layer formation and surface erosion for a single 6kV shot.

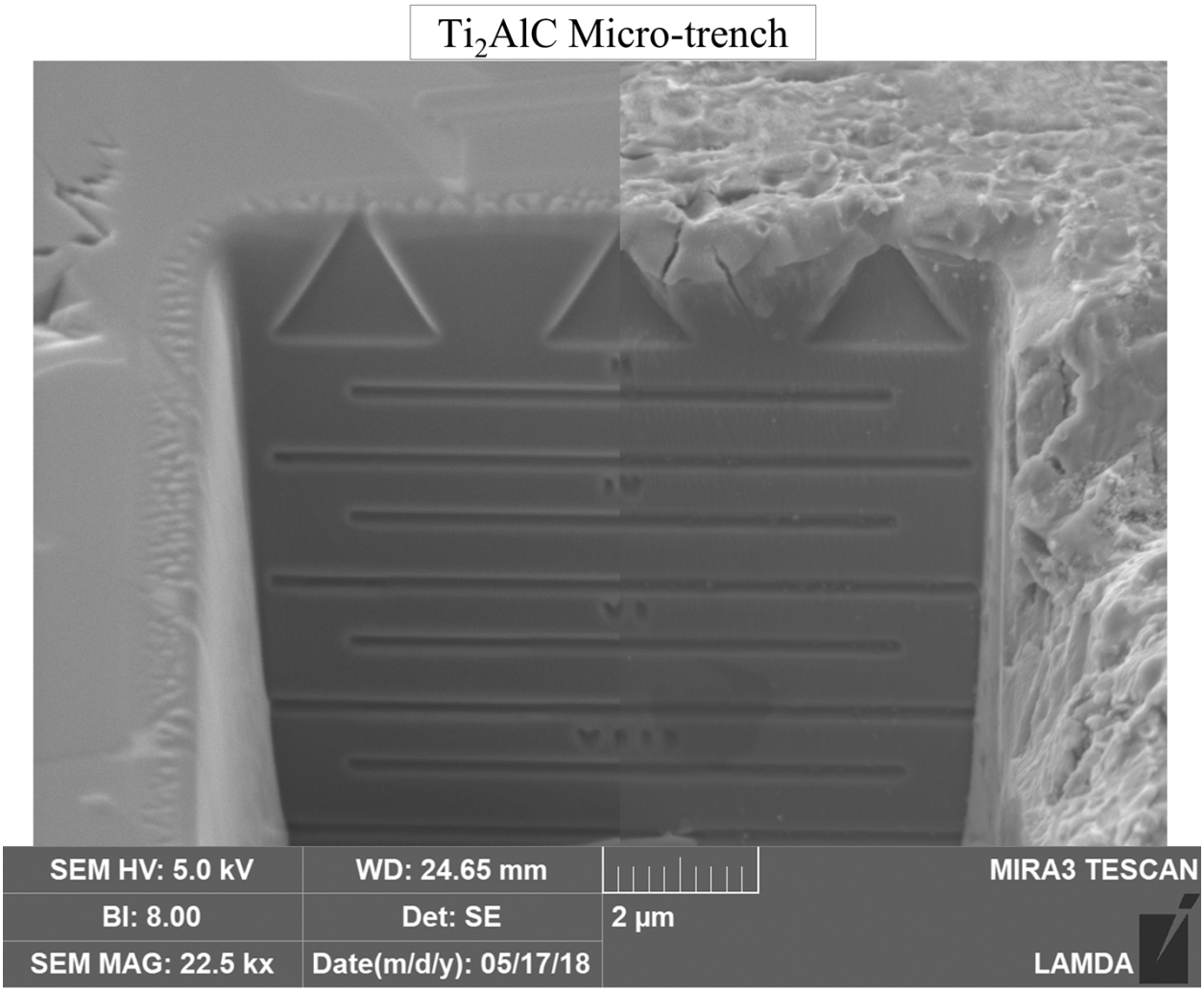

Figure 11 - Overlaid images of a Ti_2AlC micro-trench for pre-exposure (Left) and post-exposure (Right), at a 52° angle, highlighting melting and boiling along the micro-trench edge from a single 6kV plasma exposure.

In the case of 5 consecutive plasma exposures, uniform fracturing and erosion loss was observed on the sample surfaces and along the micro-trench walls. In many instances, deep fractures were observed to form along the micro-trench walls without resulting in mass material ejection. The material loss that did occur was usually contained to above the 4 μm depth marker.

As with the Ti_3SiC_2 analysis, it was important to take depth measurements for both the average surface height and the fracture depth within the micro-trench wall.

III.B.iv SiC

Three SiC samples successfully provided erosion data for the ET experiment. Two were exposed to a single plasma shot at a programmed ΔV of 6 kV and 7 kV, while the third was reserved for 5 consecutive plasma shots at 6 kV. The 3C CVD SiC was expected to exhibit low, uniform surface erosion thanks to its excellent thermal properties, strong covalent bonding, and the fact that SiC sublimates rather than melts. The SiC samples proved more robust than expected. Post-exposure surfaces showed a small increase in surface roughness, in some instances exhibiting small pits on the order of 0.2 μm in diameter. Despite the surface roughening, the FIB fiducial depth markings looked relatively unchanged after exposure; SEM image analysis, at high magnification, was necessary to confirm a small amount of surface erosion. Additionally, no surface fracturing was observed on the sample surfaces.

Low erosion thickness was observed for the two 1-shot SiC samples. One notable difference was the presence of the small, 0.2 μm pits in the lower heat flux shot. For the case of 5 ET exposures at 6kV, a similar roughened surface was seen, suggesting that any small erosion pits that formed were uniformly blended together after successive exposures. After the samples were cleaned and imaged post-experiment, there was worry that the material erosion would be too negligible to measure. The decision was made to re-expose two of the SiC samples for additional repeated plasma exposures. Even after these added exposures, negligible surface damage was observed in the SEM images. More pronounced, uniform surface roughening was present but not to the extent of the other PFMs. One sample was exposed to an additional 4 discharges at 7 kV, making for 5 total 7 kV exposures. The other sample was exposed to an

additional 10 6 kV shots, for a total of 15, resulting in a net erosion rate of 29 μm/s (±12%). This SiC sample is shown in the overlaid image in Fig. 12. The robustness of SiC to multiple 0.9 GW/ m^2 exposures is made clear in this image, displaying negligible net surface erosion and minor rounding of the micro-trench edges. This response is distinctly superior to that of the other PFMs after 1 – 5 exposures.

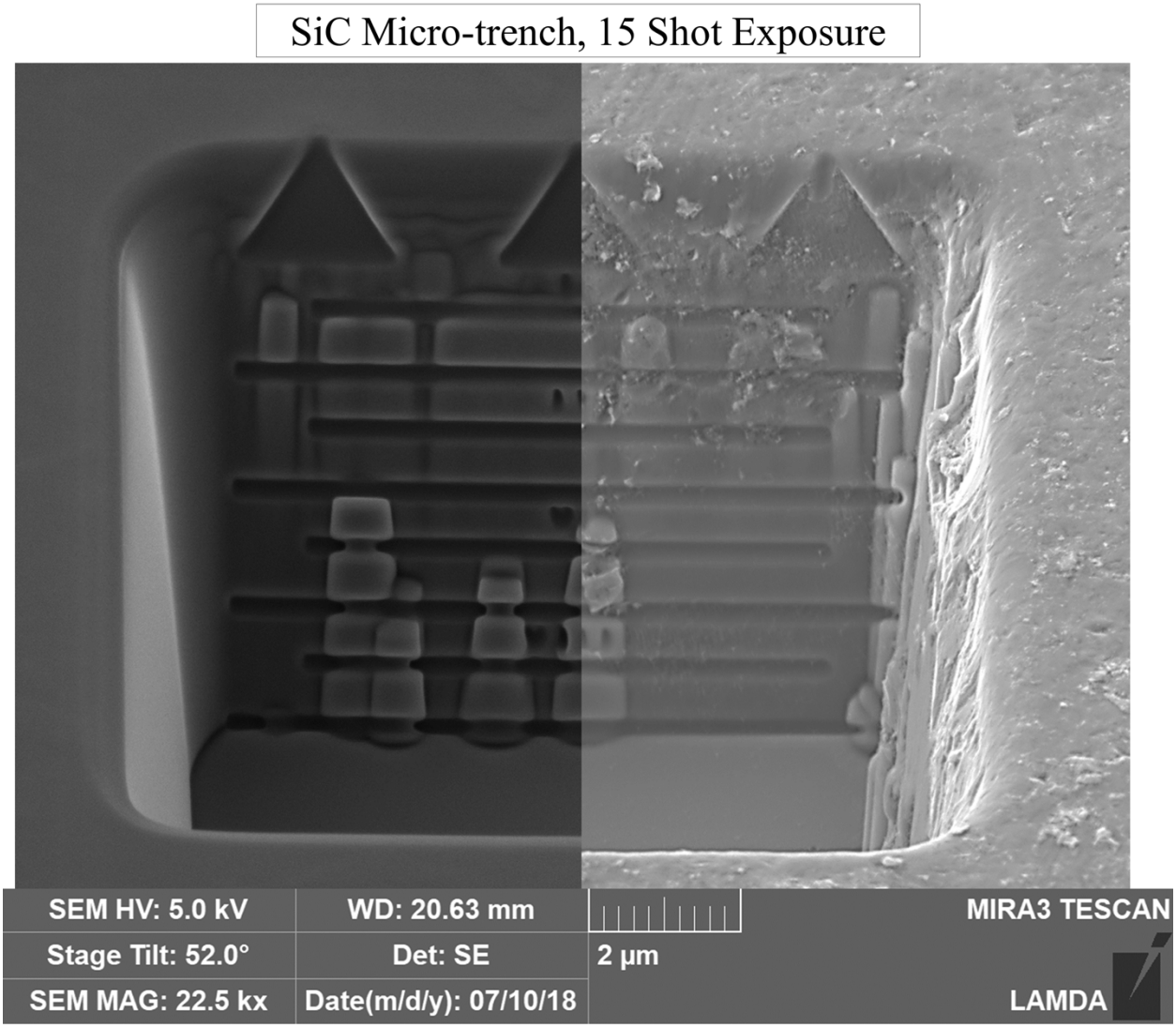

Figure 12 – Overlaid images of a SiC micro-trench for pre-exposure (Left) and post-exposure (Right), highlighting the robustness of SiC after experiencing a total of 15 ET plasma discharges at 6 kV.

III.C Results and Discussion

The total gross erosion for each material was calculated using a two-image method, combining one 0° top-down and one 52° angled image for each height measurement of interest. SEM length measurements were scaled by the scale bar provided in each image. Values for Δt_s were measured for all possible micro-trenches of each ET sample. Values for Δt_c were measured for any micro-trench that possessed melt-layer deformation or fracture within the trench wall that resulted in loss of material. Δt_c represents the maximum observed damage depth. Despite the small spread in the observed heat flux magnitudes, there was significant variation in measured gross erosion across the various micro-trench locations, implying a non-uniformity of erosion over the sample surface. For the purpose of material comparison, it is useful to focus on the maximum average erosion rate calculated at an individual micro-trench on each sample surface, with 2-3 depth measurements per micro-trench. Doing so emphasizes the worst-case scenario for each material exposure while allowing for more interpretable comparisons from the uncertain dataset.

The average surface erosion rate calculated from Δt_s is important from an erosion physics perspective and was the main driver for this experiment. The total depth of erosion damage, $\Delta t_s + \Delta t_c$, is important from an engineering perspective and equally valuable in assessing PFM performance. Measured erosion rates based on Δt_s over the 0.9 – 1 GW/m^2 heat flux range are summarized in Tables 2 and 3 below, with SiC data specifically highlighted in Table 3 for comparison with the literature. The error bars represent +/- one standard deviation for the data across an individual micro-trench. Multi-shot ET exposures often exhibited erosion rates different than the corresponding 1-shot cases since the sample surfaces roughen after each successive plasma shot. In the case of Ti_3SiC_2 and Si, the micrometer-scale surface fractures

would build up on one another and greatly increase the average erosion rate. In the case of SiC, the small sublimation pits would roughen and blend together, resulting in an overall reduced average erosion rate. Thus, it is appropriate to consider the 1-shot and multi-shot data separately. For example, the two SiC samples that were imaged and re-exposed to multiple shots provide evidence that surface roughening reduces the net erosion rate. The total, average erosion rate after 5 cumulative 7 kV exposures was 59 μm/s (±32%), while the erosion thickness loss from one 7 kV discharge was 128 μm/s (±20%). The notable sample that was exposed to a total of 15 6 kV shots registered a low net erosion rate of 29 μm/s (±12%). The comparable 1-shot 6 kV case measured an erosion rate of 91 μm/s (±30%).

Table 2 – PFM Erosion Rates Calculated From Δt_s

	Single Exposure Surface Erosion Rate (μm/s)	% error	**Multiple Exposures** Surface Erosion Rate (μm/s)	% error
Si	1210	5%	>1670	n/a
W	117	107%	32	n/a
Ti3SiC2	80 - 775	12 - 47%	584	24%
Ti2AlC	84 - 468	54%	186	7%
SiC	90 - 128	20-33%	24 - 29	12%

Table 3 – SiC Erosion Rate Data Calculated from Δt_s

SiC Sample #	Total # of Shots	Avg. Heat Flux [W/m^2]	Pulse length [s]	Erosion Depth [um]	Erosion Rate [um/s]	St. Dev. [%]
9	1	9.054E+08	0.0012	0.108811934	90.67661159	33.8%
10	5	8.911E+08	0.00116	0.136700255	23.5690095	11.9%
11	1	1.026E+09	0.0012	0.153927035	128.2725289	20.0%
9	5	9.816E+08	0.001085	0.254152788	58.56055017	32.1%
10	15	9.252E+08	0.001085	0.3188019	29.38266362	11.8%

For W, the erosion rate can be considered to be ~0 μm/s. The substantial error is due to the melt-layer motion; measurements for the new surface height depend on how the molten pits

and melt layers re-solidify after moving across the surfaces. A boiling surface temp was not reached on W. SiC was the only material to exhibit relatively uniform surface erosion across all micro-trench locations, leading to relatively consistent data. The microscopy analysis did confirm a relevant amount of erosion, 90 – 128 μm/s for the single exposures and a reduced 24 – 29 μm/s for the multiple exposures. Erosion rates for both MAX phases were inconsistent across the different micro-trench locations and shot parameters. On average, both exhibit significantly higher surface erosion rates than SiC. For the multiple exposures, Ti_3SiC_2 displayed the greatest surface erosion due to surface fracturing. Ti_2AlC, although demonstrating some surface fracturing, also formed an apparent melt layer that likely hindered some of the crack propagation. The monocrystalline Si sample displayed the highest erosion among all samples, as expected. The total depth of erosion damage, calculated from $\Delta t_s + \Delta t_c$, is displayed in Figure 13. With no melting or cracking, the erosion damage values for SiC are the same as in Table 2 and are much lower than those for the MAX phases and Si. The W values for $\Delta t_s + \Delta t_c$ are calculated based on the melt-layer depth along the micro-trench walls that might have caused material ejection. Error bars are calculated from the standard deviation for the Δt_s erosion rate measurements, since there is only one data point for Δt_c across each individual micro-trench.

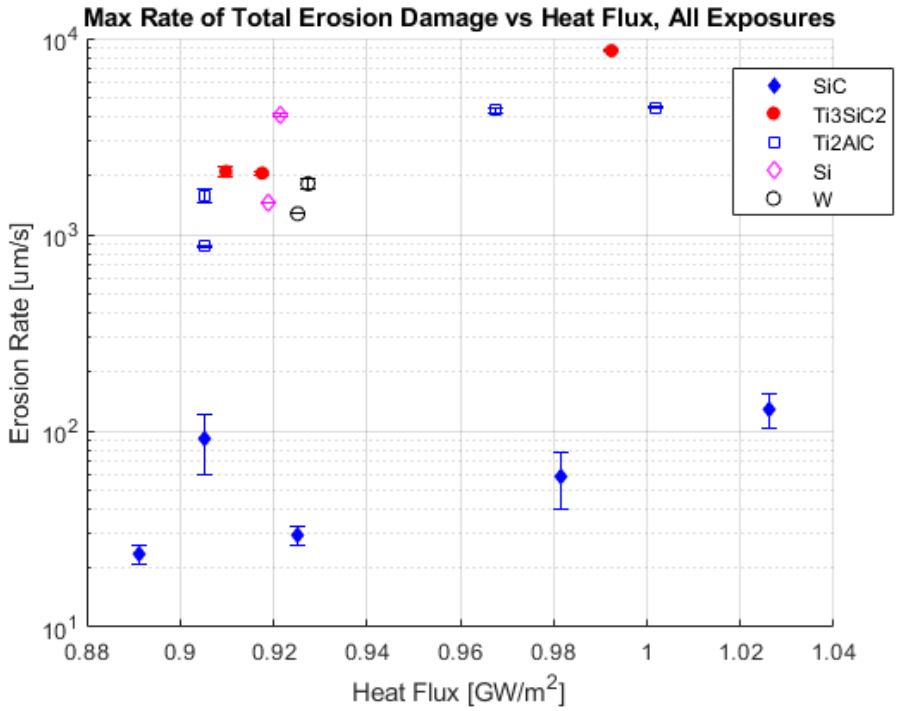

Figure 13 – Maximum erosion damage rate as a function of the average impinging heat flux, calculated from $\Delta t_s + \Delta t_c$.

W and SiC exhibited the best performance in terms of surface erosion depth. However, extreme melt-layer formation and motion was observed across the W surfaces, with deformation penetrating 1 – 7 µm deep. In the context of repeated ELMs and disruptions, this response represents a macroscopic damage risk due to microscopic melt-layer motion and material ejection. Silicon carbide exhibited stellar performance, in one case surviving 15 consecutive ET plasma exposures of about 0.9 GW/m^2 heat flux with an average erosion rate of about 26 µm/s. One possible explanation is SiC's thermal properties. The results represent the full, time-dependent materials response to ELMs/disruptions rather than erosion in an ideal 'sublimation-dominated' regime. If SiC was not elevated to its limiting temperature (~2700 °C) for as long as the other PFMs, it would exhibit a less extreme response. Both MAX phase ceramics

demonstrated poor performance in their first high heat flux plasma exposures. The MAX phase expectations were somewhat unknown. They were originally chosen as PFM candidates due to their reported thermal shock resistance. However, the high heat flux exposures were designed to test the MAX phases far past their operating temperature limits, starting from room temperature, without any active cooling. For example, rather than melting or sublimating, the MAX phases are reported to slowly dissociate. Instead, melting/boiling pits and deep surface fracturing is observed. Ti_3SiC_2 was significantly more prone to fracture and material ejection than Ti_2AlC, likely due to Ti_2AlC's better thermal conductivity and its observed melt-layer formation. Considering the surface fracture erosion mechanics, the MAX phases did not perform much better than the mono-crystalline Si. Evaluating both the erosion data and the observed material deformation mechanisms, SiC demonstrated the best performance under the high heat flux ET discharges. The overall PFM ranking is visualized in Figure 14 with side-by-side images of micro-trench erosion under five ET plasma exposures at 6 kV.

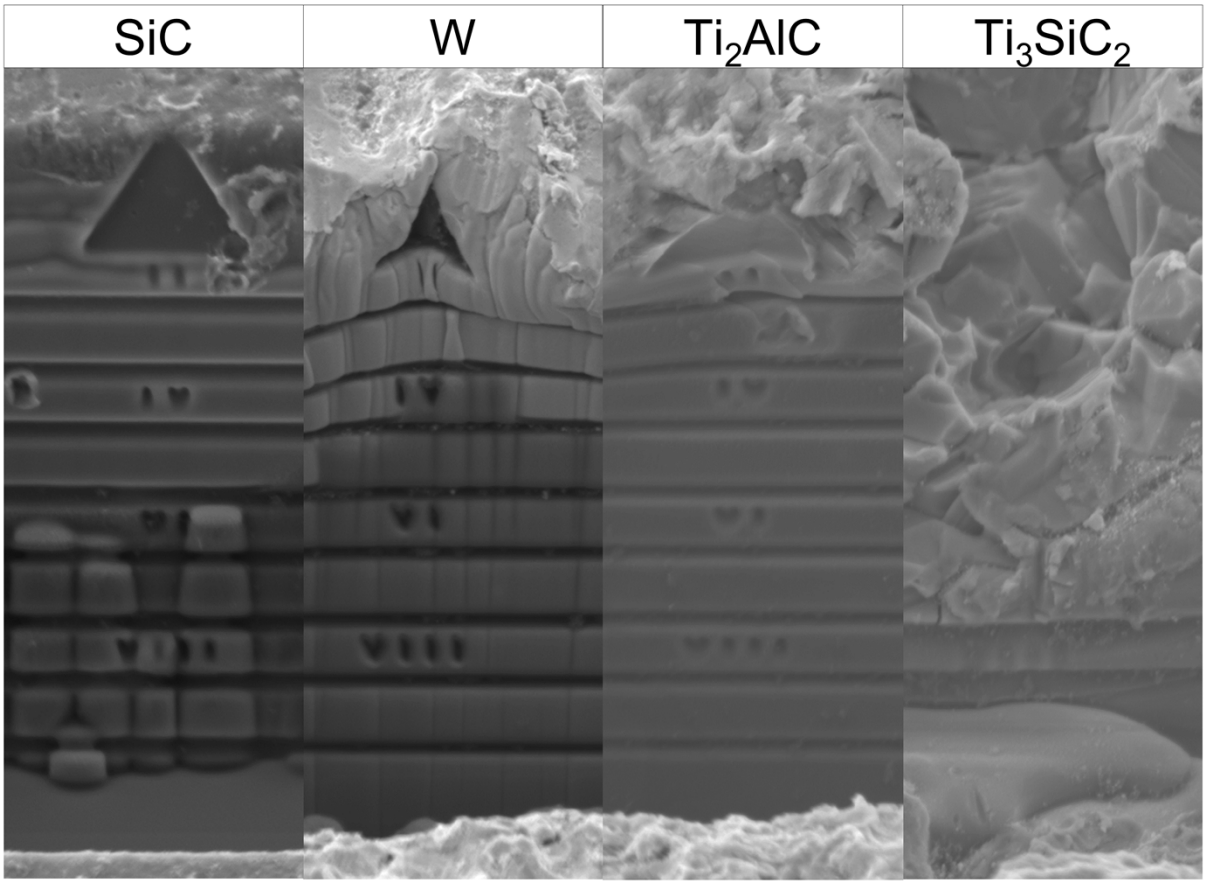

Figure 14 – Visual comparison of PFM performance from similar ET exposures, highlighting the overall PFM rankings for the study. The materials are arranged in order of best to worst performance, with SiC showing the best erosion resistance and Ti_3SiC_2 the worst erosion resistance.-

IV. Conclusions

Alternative PFM candidates Ti_3SiC_2, Ti_2AlC, and SiC were exposed for the first time to an electrothermal plasma source alongside W and Si. Samples endured single and multiple plasma exposures at 0.9 – 1 GW/m^2 over 1000 – 1200 μs. The benchmark W samples displayed little material loss but substantial melting and melt-layer motion, especially under consecutive exposures. The relatively high erosion rates for Ti_3SiC_2 and Ti_2AlC, namely due to deep surface

fracturing and material ejection, imply that both are unfit to serve as PFMs in either the divertor or first wall region. The high-purity, β-3C CVD SiC exhibited the best performance under ELM- and disruption-relevant heat loads. No surface fractures or melt deformation was observed, leading to minimal, uniform sublimation at rates of 23 – 128 μm/s. This research highlights the importance of continued exploration into alternative, reactor-relevant PFMs through evaluating new materials and developing new analysis methods. The FIB micro-trench technique successfully allowed for erosion depth measurements and provided additional insight into molten pit formation, melt-layer depth, and fracture characteristics. It is highly recommended to continue exploring well-engineered SiC materials and other ceramics that sublimate rather than melt. Further tokamak exposures, such as the complimentary experiment on DIII-D [5], are recommended to evaluate the physical sputtering erosion response under ~MW/m^2 conditions. This type of study would be well complemented by plasma exposures on linear devices, such as Proto-MPEX/MPEX at ORNL, so long as the exposure conditions match plasma impacts within a tokamak. For SiC in particular, a simultaneous test of the high-purity β-3C CVD with SiC/SiC composites would be valuable, as that material was not acquired for this study. As for the MAX phase ceramics, if they are again tested, it is highly recommended to test new MAX phases, with improved thermal properties, under heated conditions.

This material is based upon work supported by the U.S. Department of Energy via UT Batelle, LLC Subcontract 4000145506. CMP supported by an Early Career Award, US Department of Energy, Office of Science, Fusion Energy Sciences, under contract number DE-AC05-00OR22725. This work was performed in part at the Analytical Instrumentation Facility (AIF) at North Carolina State University, as well as the Low Activation Materials Development and Analysis (LAMDA) laboratory at Oak Ridge National Laboratory [25].

References

[1] R.A. PITTS et al. "A Full Tungsten Divertor for ITER: Physics Issues and Design Status," *Journal of Nuclear Materials*, **438** (2013) S48-S56

[2] M. MEROLA et al. "ITER Plasma-facing components," *Fusion Engineering and Design*, **85** (2010) 10-12

[3] R.A. PITTS et al. "Physics Basis and Design of the ITER Plasma-Facing Components," *Journal of Nuclear Materials*, **415**, S957 (2011)

[4] M. KIKUCHI et al. *Fusion Physics*, Chap. 7, p. 834, Vienna (2012)

[5] J. COBURN et al. "Erosion Characterization of SiC and Ti_3SiC_2 on DIII-D using Focused Ion Beam Micro-Trenches," Presentation, 23rd International Conference on Plasma Surface Interactions in Controlled Fusion Devices (PSI-23), to be published in Nuclear Materials and Energy

[6] M. BARSOUM, MAX Phases: Properties of Machinable Ternary Carbides and Nitrides, Wiley-VCH Verlag GmbH & Co, 2013

[7] D.J. TALLMAN et al. "Effect of Neutron Irradiation on Select MAX Phases," *Acta Materialia,* **85**, 132 (2015)

[8] D.W. CLARK et al. "High Temperature Ion Irradiation Effects in MAX Phase Ceramics," *Acta Materialia*, **105**, 130 (2016)

[9] D.J. TALLMAN et al. "Effects of neutron irradiation of Ti3SiC2 and Ti3AlC2 in the 121-1805 C temperature range," *Journal of Nuclear Materials*, **484** (2017) 120-134

[10] L.L. SNEAD et al. "Silicon Carbide Composites as Fusion Power Reactor Structural Materials," *Journal of Nuclear Materials*, **417**, 330 (2011)

[11] L.L. SNEAD et al. “Handbook of SiC Properties for Fuel Performance Modeling,” J*ournal of Nuclear Materials*, **371**, 329 (2007)

[12] IVEKOVIC et al., “Current status and prospects of SiCf/SiC for fusion structural applications,” *Journal of the European Ceramic Society*, **33** (2013) 10

[13] Y. KATOH et al. “Current Status and Recent Research Achievements in SiC/SiC Composites”, *Journal of Nuclear Materials*, **455** (2014) 387-397

[14] Rohm & Haas CVD Silicon Carbide Data Sheet, 2008

[15] T.E. Gebhart et al. “Material impacts and heat flux characterization of an electrothermal plasma source with an applied magnetic field,” *Journal of Applied Physics*, **122**, 063302 (2017)

[16] M. A. Bourham, O. E. Hankins, O. Auciello, J. M. Stock, B. W. Wehring, R. B. Mohanti, J. G. Gilligan, “Vapor Shielding and Erosion of Surfaces Exposed to a High Heat Load in an Electrothermal Accelerator,” *IEEE Transactions on Plasma Science*, **17**, No. 3, (1989)

[17] A. L. WINFREY et al. “A Study of Plasma Parameters in a Capillary Discharge with Calculations Using Ideal and Nonideal Plasma Models for Comparison With Experiment,” *IEEE Transactions on Plasma Science*, **40**, 843 (2012)

[18] J.G. Gilligan and M.A. Bourham, “The use of an Electrothermal Plasma Gun to Simulate the Extremely High Heat Flux Conditions of a Tokamak Disruption,” *Journal of Fusion Energy*, **12,** (1993) 311-316

[19] R. KHAZIEV and D. CURRELI, “Ion energy-angle distribution functions at the plasma-material interface in oblique magnetic fields,” *Physics of Plasmas*, **22**, 043503 (2015)

[20] I. BORODKINA et al. “An Analytical Expression for the Electric Field and Particle Tracing in Modelling of Be Erosion Experiments at the JET ITER-like Wall”, *Contrib. Plasma Phys.* **56**, No. 6-8, (2016) 640 – 645

[21] N. M. Almousa, J. G. Gilligan and M. Bourham, "Surface Ablation and Melting of Fusion Materials Simulated by Transient High Heat Flux Generated in an Electrothermal Plasma Source," *IEEE Transactions on Plasma Science*, **44**, 9, (2016) 1642-1648

[22] H. Maier et al. “Erosion Behavior of Actively Cooled Tungsten Under H/He High Heat Flux Load”, *Journal of Nuclear Materials*, **438** (2013) S921-S924

[23] A. Litnovsky et al. “Smart Alloys for a Future Fusion Power Plant: First Studies Under Stationary Plasma Load and in Accidental Conditions”, *Nuclear Materials and Energy*, **12** (2017) 1363 – 1367

[24] “Emissivity Values,” Optotherm Thermal Imaging, https://www.optotherm.com/emiss-table.htm Accessed 15 Aug. 2018

[25] Parish CM et al. “LAMDA: irradiated-materials microscopy at Oak Ridge National Laboratory,” Microscopy and Microanalysis. V21(Suppl. 3): P.1003 (2015)